The influence of musculoskeletal forces on the growth of the prenatal cortex in the ilium: a finite element study

Peter J. Watson, Michael J. Fagan and Catherine A. Dobson

Medical and Biological Engineering Research Group, Department of Engineering, University of Hull, Hull, HU6 7RX, UK

Corresponding author: Peter J. Watson, Medical and Biological Engineering Research Group, Department of Engineering, University of Hull, Hull HU6 7RX, UK

Tel: +441482 466319; Email: p.j.watson@hull.ac.uk

This is an Accepted Manuscript of an article published by Taylor & Francis in Computer Methods in Biomechanics and Biomedical Engineering on 13 Jun 2020, available online: https://doi.org/10.1080/10255842.2020.1777546

Abstract

Remodelling and adaptation of bone within the pelvis is believed to be influenced by the mechanical strains generated during locomotion. Variation in the cortical bone thickness observed in the prenatal ilium has been linked to the musculoskeletal loading associated with *in utero* movements; for example the development of a thicker gluteal cortex is a possible response to contractions of the gluteal muscles. This study examines if the strains generated in the prenatal iliac cortex due to musculoskeletal loading *in utero* are capable of initiating bone remodelling to either maintain homeostasis or form new bone. Computational modelling techniques were used firstly to predict the muscle forces and resultant joint reaction force acting on the pelvis during a range of *in utero* movements. Finite element analyses were subsequently performed to calculate the von Mises strains induced in the prenatal ilium. The results demonstrated that strains generated in the iliac cortex were above the thresholds suggested to regulate bone remodelling to either maintain homeostasis or form new bone. Further simulations are required to investigate the extent to which the heterogeneous cortex forms in response to these strains (i.e. remodelling) or if developmental bone modelling plays a more pivotal role.

Introduction

The remodelling of bone is believed to follow the "mechanostat" model of bone regulation (Frost, 2003), whereby bone is either formed or resorbed in response to the mechanical strains that it experiences. Based on this theory, it has been suggested that the internal architecture of the pelvis remodels in order to align with the principal strain trajectories associated with bi-pedal locomotion (Macchiarelli et al., 1999; Rook et al., 1999).

This functional relationship has also been used to explain the ontogenetic development of trabecular bone in the femur and tibia. For example, the gradual remodelling of trabeculae in juveniles to eventually form the structural organisation observed in adults, has been related to the strain experienced during locomotive development (Gosman and Ketcham, 2009; Ryan and Krovitz, 2006). However, interestingly the pelvis is reported to contain a high level of structural optimisation at very young ages, with an adult-like trabecular organisation observed *in utero* (Cunningham and Black, 2009a, 2009b) and heterogeneous cortical thickness present in the neonate (Cunningham and Black, 2009c).

The surprising presence of such structural optimisation in the fetal pelvis could be due to bone modelling, which possibly contains a genetic blueprint of the partially optimised structures. Alternatively, it has been suggested that fetal kicks against the uterine wall may provide a form of resistance training (Land and Schoenau, 2008; Rauch and Schoenau, 2001). Hence this partial optimisation could be in response to musculoskeletal loading *in utero* (Cunningham and Black, 2010, 2009a, 2009b). For example, the thicker cortex on the gluteal surface has been linked to the action of the gluteal muscles (Cunningham and Black, 2009c).

If musculoskeletal loading *in utero* does play a key role in the growth of a heterogeneous cortical thickness in the neonatal pelvis, it would be expected that strains within the cortex would be large enough to initiate bone remodelling to either maintain homeostasis or form new bone. Finite element (FE) analysis of a 30 week old mineralized pelvis has shown that some regions do experience

strains capable of initiating bone remodelling, when considering forces associated with fetal kicking (Verbruggen et al., 2018). However, it remains unclear if these forces are responsible for the formation of the partially optimised trabecular and cortical structures in the pre and neonatal pelvis.

Here, we use computational modelling to investigate whether the musculoskeletal loading *in utero* generates strain magnitudes which are capable of initiating bone remodelling to either maintain homeostasis or form new bone in the pelvic cortex. This was undertaken through the use of a musculoskeletal model (MSM) of the prenatal hip joint to predict the mechanical loading associated with fetal movement, with subsequent FE analyses then calculating the resulting bone strains.

Methods

Digitised modelling – A dry prenatal pelvic specimen belonging to the Scheuer Collection repository of juvenile remains (University of Dundee, UK) was selected for analysis. This specimen contained a fully articulated pelvic gridle and was checked visually for structural abnormalities. It was scanned using an X-TEK HMX160 micro-computed tomography (µCT) system (X-Tek Systems Ltd, UK) with a resolution of 58.8µm. Scan data were digitised in AVIZO v9.5 (Visualization Sciences Group Inc., USA) to provide a volumetric model of the pelvic girdle. This model was used to measure the iliac and ischial width and length, along with the pubis length. Based on the anthropometric data of Fazekas and Kosa (1978) the gestational age of the specimen was estimated to be 34-38 weeks. Due to the symmetric nature of the pelvis about the mid-plane, only the right hemi-pelvis was selected for further modelling.

The prenatal specimen did not possess all the triradiate cartilage of the acetabular corpus (Fig. 1a), therefore a reconstruction technique, based on geometric morphometric methods (Watson et al., 2011), was applied to reconstruct the complete acetabular structure. A landmark configuration consisting of 34 landmarks covering the entire hemi-pelvic structure was manually defined based on identifiable anatomical features (Fig. 1b). This configuration used the same landmarks described in Watson et al. (2011), with additional landmarks defined round the exterior of the acetabulum. A CT scan of a 19 year old hemi-pelvis was then digitised into a volumetric model and the same landmark configuration then replicated on this fused structure. These landmarks were then used to create a

template of appropriate form (size and shape), using warping tools (a triplet of thin plate splines – the 'Bookstein' function (Bookstein, 1989)) within AVIZO to warp the 19 year old hemi-pelvis to fit the estimated size and shape of the prenatal hemi-pelvis landmark configuration. This created a warped template which superimposed that of the prenatal hemi-pelvis and provided an estimate of the missing triradiate cartilage. Using the contours of the warped template in the regions of the missing triradiate cartilage, a complete prenatal acetabulum was then reconstructed (Fig. 1c).

Musculoskeletal modelling – A MSM of the prenatal hip was created in AnyBody v7.1 (AnyBody Technology, Denmark) to predict the muscle and hip joint reaction forces associated with *in utero* movements. The joint was modelled in the fetal position, which is characterised by hyper flexion of the hip joint (Shefelbine and Carter, 2004). The corresponding femur to the prenatal hemi-pelvis was not available, therefore an adult femur was scaled down to an appropriate size, as determined by the anthropometrics reported by Fazekas and Kosa (1978). Although the geometry of this scaled femur inevitably differs in some respects to that of an actual prenatal femur, it provided a reasonable estimate which was only required to define the locations of the muscle attachments. The prenatal hemi-pelvic and femoral volumetric models were input to AnyBody and connected through a spherical joint. The weight of a 36 week old fetus was estimated at 2.6Kg (Salomon et al., 2007) and subsequently used to calculate the individual limb weights via the anthropometric data of Winter (1990). The weight of the lower limb distal to the knee was applied at the mid-point between the medial and lateral femoral epicondyles.

The origin and insertion of 21 muscles spanning the hip joint were identified in accordance with Scheuer and Black (2000). Muscles attaching to the tibia or fibula were modelled as terminating at the point at which they wrapped around the distal femur (i.e. epicondyles or patella). The coordinates of muscle attachments to the patella were estimated based on the proportions of the distal femur. Larger muscles were modelled with numerous strands which spanned their broad origin/attachment sites (Fig. 2a, Table 1).

The hip joint was set to 110° flexion in order to replicate the fetal position, and a rotational driver applied to simulate limb twitching in four separate movements: 5° flexion; 5° extension; 5° adduction; and 5° abduction (Fig. 2b & c). To model interaction between the knee and uterine wall, a resistive force which increased linearly to the femoral movement was applied to the distal femur. The force generated by the knee on the uterine wall at 34-38 weeks gestation is unknown, but it was assumed to be lower than the 17N reported for kicking by the full lower limb at this gestational age (Verbruggen et al., 2018). Hence, with the femur estimated to account for 62% of the total lower limb mass, the 17N force was scaled to account for just the mass of the femur. Consequently, the resistive force was defined so that the full 5° (in all movements) had to overcome a maximum resistance of 10.54N.

To maintain the kinematic determinacy of the model, a rigid constraint was applied at the sacro-iliac joint (SIJ). Joint and muscle kinetics were computed through an inverse dynamics analysis (Table 1) using a pre-defined cubic solver which minimises the sum of the cubed muscle activations. Like many recruitment solvers used in MSMs, this solver may recruit a muscle if it has a positive moment arm and the force generated contributes to the motion, irrespective of the muscle's primary function. As a result, Table 1 shows that some muscles are active during movements even though this may not be conventionally associated with their primary function. For example the rectus femoris, which has a primary function of flexion, was predicted to contribute to flexion, adduction and abduction. In addition, some muscles, such as the adductor brevis and gluteus maximus were not active during their primary tasks because their moment arms did not assist in the desired motion at the high flexion angle considered.

Finite Element Modelling - The volumetric model of the prenatal hemi-pelvis (Fig. 1c) was meshed in AVIZO to produce a total of ~1.53 million 10-noded tetrahedral elements, representing the trabecular bone and triradiate cartilage. The mesh was subsequently imported to ANSYS v2019 R3

(ANSYS Inc., USA), where 84,476 shell elements were clad around the bony structure to represent the cortical bone.

Information on the material properties of prenatal pelvic bone is scarce, therefore the Young's modulus (E) of cortical bone was defined as 7.02GPa (Kim et al., 2016), with a Poisson's Ratio (ν) of 0.3. The modulus of trabecular bone was estimated using the non-linear relationship $E_{Trabecular} = 1.24\ E_{Tissue}\ (BV/TV)^{1.8}$ (Yang et al., 1998), where E_{Tissue} was set equal to $E_{Cortical}$. The BV/TV calculated previously for this specimen was 28.31% (Cunningham and Black, 2009b), therefore $E_{Trabecular}$ was estimated to be 898MPa (ν = 0.2). Triradiate cartilage was defined as E = 25MPa (ν = 0.4) (Dong et al., 2013).

Unfortunately, the true heterogeneity of the cortical thickness could not be ascertained accurately from the μCT scan data. Therefore, a uniform grid which replicated the size and position of a similar grid used by Cunningham and Black (2009c), was defined on the ilium to divide the pelvic and gluteal surfaces into small regions of interest (ROIs) (Fig. 3). A heterogeneous cortex was then modelled by creating shell elements over each ROI and defining a thickness which corresponded to the values reported by Cunningham and Black (2009c) (Fig 3). However, they did not analyse small regions around the iliac crest and the posterior limit of the ilium, hence estimations of the cortical thickness in these regions were based on their neighbouring ROIs. In addition, while the location of the pelvic ROIs closely matched the grid used by Cunningham and Black (2009c), some gluteal ROIs were extended to ensure they reached the acetabular rim. This was due to a slight variation in the acetabular morphology between the specimen modelled here and the neonatal specimens analysed by Cunningham and Black (2009c). Consequently, the pelvic surface was characterised through an additional ROI compared to the gluteal surface (Fig. 3). Data for the cortical morphology of the ischium and pubis are not available, hence a constant value of 0.6mm (the average iliac cortical thickness) was applied to shell elements on each bone.

The data of Cunningham and Black (2009c) was considered suitable for this study due to the estimated age of the specimen modelled (i.e. close to term) and the fact that reduced musculoskeletal loading immediately after birth (Land and Schoenau, 2008) limits the potential for significant alterations in neonatal bone morphologies.

Muscle forces were applied as distributed loads over their attachment areas and were defined in according to the muscle representation of the MSM as described above (i.e. broad origins were modelled in more than one section). The hip joint reaction force was distributed uniformly in a radial direction over the nodes of the acetabulum. The area of articulation within the SIJ was extruded medially by a thickness of 1.3mm (the average thickness of the SIJ cartilage measured at 20 locations through the structure) and meshed with 60,371 10-noded tetrahedral elements, and defined with the material properties of cortical bone. Ten nodes around the circumference of the medial surface of the extruded area were constrained in all DOF to enable the hemi-pelvis to rotate about the extrusion, thus simulating pelvic rotation about the SIJ.

The model was analysed four times; once for each of the loading regimes calculated by the MSM (i.e. flexion, extension, adduction and abduction). The von Mises strains generated by the four load regimes were initially stored in separate element tables, with a cumulative, peak element table then created by selecting the largest von Mises strain in each element from any of the four loading regimes. This peak element table was subsequently plotted to reveal the maximum von Mises strain experienced across the ilium for the range of hip joint movements.

Results

The von Mises strain distributions generated by flexion and adduction display similar characteristics (Fig. 4). On the pelvic surface, strains above 1000$\mu\varepsilon$ are positioned around the SIJ and dissipate in two superiorly directed trajectories; one through the fossa travelling towards the iliac crest and another towards the posterior region of the ilium. On the gluteal surface, high strains (>1000$\mu\varepsilon$)

concentrate around the greater sciatic notch and dissipate anteriorly towards the lesser sciatic notch, leaving much of the superior iliac blade under lower strain (<500με). High strains are also observed in the acetabulum.

In comparison the strains generated during extension and abduction are much lower and result in large areas of the ilium experiencing strains below 500με. However, a small area of large strain (>1000με) is observed around the SIJ during abduction, while the inferior ilium and acetabulum experienced high strains during extension.

The distribution produced when plotting the overall peak von Mises strain in each element arising from the four hip joint movements (Fig. 5) (hereafter referred to as peak strain) resembles that associated with flexion and adduction (Fig. 4). However strains are observed between the acetabulum and greater sciatic notch on the pelvic surface, which resembles that generated during extension.

Discussion

The FE analyses have shown that 99.7% of the total iliac surface area experience peak von Mises strains (Fig. 5) above the threshold required for bone remodelling to maintain homeostasis (100με, (Frost, 2003)). The location of peak strains above the threshold suggested to initiate bone formation (1500με, (Martin, 2000)) are consistent with the regions containing the thickest cortex, namely around the greater sciatic notch and the trabecular chiasma (Cunningham and Black, 2009c).

On the gluteal surface the peak strains dissipate primarily in an anteriorly directed trajectory (Fig. 5), however this is not consistent with the morphology of the gluteal cortex which reduces in thickness in a radial pattern from the greater sciatic notch (Cunningham and Black, 2009c). The lack of strain dissipation in the superior regions could be linked to the development of a relatively thicker cortex in the gluteal surface, when compared to that of the pelvic surface (Fig. 3). Cunningham and Black (2009c) suggest this is in response to the loading of the gluteal muscles. This study is unable to

confirm this as the MSM predicted low activity of the gluteal muscles for the movements simulated (with the exception of the gluteus medius during abduction) (Table 1). Nevertheless, even with low activation of the gluteal muscles, the peak strains in the region of the gluteal attachments are between 100-1500$\mu\varepsilon$, indicating that bone remodelling is maintaining homeostasis (Martin, 2000) in order to maintain the thicker cortex to resist the muscle loading. The high peak strains generated near the lesser sciatic notch on both surfaces are attributed to the low thickness of the cortex in this region (Fig. 3) combined with the origin of the rectus femoris, which produces a high force during flexion and adduction (Table 1).

The thickness of the pelvic cortex is known to reduce superiorly (Cunningham and Black, 2009c), and this generally correlates with the trajectories of the dissipating peak pelvic strains (Fig. 5). Although it might be expected that the regions around the SIJ would contain thicker bone to mitigate the high strains, the superior regions have had less time to undergo remodelling when compared to the inferior regions because iliac growth radiates from the nutrient foramen (Cunningham and Black, 2009c). Therefore, it is possible that the specimen modelled here has not yet adapted to the musculoskeletal forces experienced on the pelvic surface.

Fig. 5 illustrates that peak strains in the ilium due to musculoskeletal loading *in utero* are sufficiently high in areas to initiate bone formation, or at least maintain homeostasis across the whole structure. Regions that experience strains above the threshold suggested for bone formation (1500 $\mu\varepsilon$) account for 25.4% of the total iliac surface area, demonstrating that some areas of the structure have yet to fully optimise to the musculoskeletal loading. These *in silico* results suggest that *in utero* loading is capable of initiating bone remodelling to maintain the heterogeneous morphology of the iliac cortex.

The peak strains are predominantly caused by adduction, which accounts for 79.9 % of the peak strains illustrated in Fig. 5 (flexion, extension and abduction account for 7.4%, 5.7% and 7.0 %, respectively). The peak strains are representative of the forces predicted by the MSM. These forces

are influenced by the resistance applied to the movements simulated (although the actual resistance provided by the uterine wall to the knee may vary) and the definition of the muscle line of action. The resistance applied at the knee in the MSM was deemed reasonable for flexion and extension, although could be too high for adduction and abduction. Lowering the resistance to adduction and abduction to 5N did significantly lower the contributions of these movements to the peak strains (89.9% flexion, 8.4% extension, 0.1% adduction and 1.6% abduction). As the contribution from adduction was lower, the resulting distribution of peak strains primarily resembled that generated by flexion (Fig 4). Therefore, this produced only a minor alteration to the distribution of the peak strains when compared to Fig. 5, and thus did not influence the observations made above. The muscle wrapping defined in the MSM affects the muscle moment arms at the high flexion angle simulated, causing redundancy in some muscles during movements which are considered their primary task. The positioning of the muscle wrapping is open to operator interpretation of the correct muscle excursions at the high flexion angle modelled. Unfortunately, the muscle excursions in the MSM cannot be validated due to the lack of data concerning muscle paths at the prenatal hip with high flexion angles.

It is important to comment that this study presents predicted strains, and due to the obvious difficulties in measuring *in vivo* strains associated with *in utero* movements, these results cannot be validated. In addition, there are assumptions in this study which should also be considered when interpreting the results; in particular, the strain remodelling thresholds and the modelling simplifications. The results only demonstrate that the strains are large enough to initiate bone remodelling based on a single load and time point and suggested physiological strain thresholds (Frost, 2003; Martin, 2000). Therefore, this study does not consider the strain rate associated with *in utero* loading, which is known to be a primary driver of bone remodelling (Turner, 1998) and can alter the threshold that initiates bone formation (Hsieh and Turner, 2001). Further investigations are required to determine the strain rate associated with muscle contractions *in utero*, and the extent to

which the heterogeneous cortex forms in response to these strain rates (i.e. remodelling), or if developmental bone modelling plays a more pivotal role.

Homogenous material properties were used, but material properties for prenatal tissue are scare, hence this was unavoidable. Furthermore, because the FE model did not contain ligaments, the triradiate cartilage was modelled with a slightly higher stiffness to provide additional stability to the large cartilaginous structure (Fig. 1). A range of stiffness values for triradiate cartilage and growth plates are reported in the literature, and therefore a sensitivity test was performed with a lower modulus (E = 5MPa, ν = 0.495) (Pinheiro et al., 2018) to assess this simplification. This resulted in greater movement of the ischial-pubic structure, but 99.8% of the total iliac surface area still experienced peak strains above 100$\mu\varepsilon$ (with 27.5% of the surface experiencing strains above 1500$\mu\varepsilon$). Adduction was still the main contributor to the peak strains, therefore the distribution of the peak strains across the ilium was similar to Fig 5. Hence assuming a lower modulus did not influence the above observations.

Another simplification regards the morphology of the prenatal structure. The morphometric reconstruction technique estimated the cartilaginous acetabulum using a template based on an adult pelvis (Fig. 1). However, the geometry and location of the prenatal bones remained unchanged and the hip joint reaction force was applied in a radial direction over the inside of the acetabulum, so that the resultant force acted in the correct direction. The modelling of the cortex in small ROI results in step changes of thickness across the iliac surface. This causes some disruption to the strain distributions, as evident around the anterior superior iliac spine on the gluteal surface in Fig. 5. Introducing a gradual change in thickness between each ROI would alter the proportion of the surface above the 100$\mu\varepsilon$ and 1500$\mu\varepsilon$ strain thresholds slightly, however this would not affect the observations made regarding the overall strain distributions.

Acknowledgements

The authors would like to acknowledge Sue Black (Lancaster University) and Craig Cunningham (University of Dundee) for providing access to the Scheuer Collection and advice regarding pelvic juvenile ontogeny, and Sebastian Dendorfer (OTH Regensburg) for providing advice on musculoskeletal modelling.

Conflict of interest statement

The authors declare that there is no conflict of interest regarding the content of this article.

References

Bookstein, F.L., 1989. Principal Warps: Thin-Plate Splines and the Decomposition of Deformations. IEEE Trans. Pattern Anal. Mach. Intell. 11, 567–585.

Cunningham, C. a, Black, S.M., 2010. The neonatal ilium-metaphyseal drivers and vascular passengers. Anat. Rec. (Hoboken). 293, 1297–309.

Cunningham, C.A., Black, S.M., 2009a. Anticipating bipedalism: Trabecular organization in the newborn ilium. J. Anat. 214, 817–829.

Cunningham, C.A., Black, S.M., 2009b. Development of the fetal ilium - Challenging concepts of bipedality. J. Anat. 214, 91–99.

Cunningham, C.A., Black, S.M., 2009c. Iliac cortical thickness in the neonate - The gradient effect. J. Anat. 215, 364–370.

Dong, L., Li, G., Mao, H., Marek, S., Yang, K.H., 2013. Development and validation of a 10-year-old child ligamentous cervical spine finite element model. Ann. Biomed. Eng. 41, 2538–2552.

Fazekas, I.Gy., Kosa, F. 1978. Forensic Fetal Osteology. Budapest: Akademiai Kiado.

Frost, H.M., 2003. Bone's Mechanostat: A 2003 Update. Anat. Rec. 275A, 1081-1101.

Gosman, J.H., Ketcham, R.A., 2009. Patterns in ontogeny of human trabecular bone from sunWatch village in the prehistoric ohio valley: General features of microarchitectural change. Am. J. Phys. Anthropol. 138, 318–332.

Hsieh, Y.-F., Turner, C.H., 2001. Effects of loading frequency on mechanically induced bone formation. J. Bone Miner. Res. 16, 918–924.

Kim, G., Elnabawi, O., Shin, D., Pae, E.-K., 2016. Transient Intermittent Hypoxia Exposure Disrupts Neonatal Bone Strength. Front. Pediatr. 4:15.

Land, C., Schoenau, E., 2008. Fetal and postnatal bone development: reviewing the role of mechanical stimuli and nutrition. Best Pract. Res. Clin. Endocrinol. Metab. 22, 107–118.

Macchiarelli, R., Bondioli, L., Galichon, V., Tobias, P. V, 1999. Hip bone trabecular architecture shows uniquely distinctive locomotor behaviour in South African australopithecines. J. Hum. Evol. 36, 211–232.

Martin, R.B., 2000. Toward a unifying theory of bone remodeling. Bone 26, 1–6.

Pinheiro, M.D.S., Dobson, C., Clarke, N.M., Fagan, M., 2018. The potential role of variations in juvenile hip geometry on the development of Legg-Calvé-Perthes disease: a biomechanical investigation. Comput. Methods Biomech. Biomed. Engin. 21, 194–200.

Rauch, F., Schoenau, E., 2001. The developing bone: Slave or master of its cells and molecules? Pediatr. Res. 50, 309–314.

Rook, L., Bondioli, L., Köhler, M., Moyà-Solà, S., Macchiarelli, R., 1999. Oreopithecus was a bipedal ape after all: Evidence from the iliac cancellous architecture. Proc. Natl. Acad. Sci. U. S. A. 96, 8795–8799.

Ryan, T.M., Krovitz, G.E., 2006. Trabecular bone ontogeny in the human proximal femur. J. Hum. Evol. 51, 591–602.

Salomon, L.J., Bernard, J.P., Ville, Y., 2007. Estimation of fetal weight: Reference range at 20-36 weeks' gestation and comparison with actual birth-weight reference range. Ultrasound Obstet. Gynecol. 29, 550–555.

Scheuer, L., Black, S. 2000. Developmental Juvenile Osteology. 1st ed. Academic Press. United Kingdom.

Shefelbine, S.J., Carter, D.R., 2004. Mechanobiological predictions of growth front morphology in developmental hip dysplasia. J. Orthop. Res. 22, 346–352.

Turner, C.H., 1998. Three rules for bone adaptation to mechanical stimuli. Bone 23, 399–407.

Verbruggen, S.W., Kainz, B., Shelmerdine, S.C., Hajnal, J.V., Rutherford, M.A., Arthurs, O.J., Phillips, A.T.M., Nowlan, N.C., 2018. Stresses and strains on the human fetal skeleton during development. J. R. Soc. 15: 20170593.

Watson, P.J., O'Higgins, P., Fagan, M.J., Dobson, C.A., 2011. Validation of a morphometric reconstruction technique applied to a juvenile pelvis. Proc. Inst. Mech. Eng. Part H J. Eng. Med. 225, 48–57.

Winter, D.A. 1990. Biomechanics and Motor Control of Human Movement, 2nd ed. United States. John Wiley & Sons.

Yang, G., Kabel, J., Van Rietbergen, B., Odgaard, A., Huiskes, R., Cowin, S.C., 1998. Anisotropic Hooke's law for cancellous bone and wood. J. Elast. 53, 125–146.

		Force (N)			
Muscle	**No. of strands**	**Flexion**	**Extension**	**Adduction**	**Abduction**
Adductor Brevis	1	-	-	-	-
Adductor Magnus	3	5.2	6.5	32.1	-
Adductor Longus	1	-	5.9	-	-
Biceps Femoris	1	-	17.5	-	13.1
Gemellus Inferior	1	-	-	-	1.3
Gemellus Superior	1	5.1	0.9	8.6	1.7
Gluteus Maximus	1	-	-	-	-
Gluteus Medius	3	-	5.9	-	27.8
Gluteus Minimus	3	-	0.8	-	2.7
Gracilis	1	8.7	1.8	22.1	-
Iliacus	3	12.1	-	28.2	-
Obturator Externus	2	-	-	-	-
Obturator Internus	2	2.0	4.5	-	16.4
Pectineus	1	5.1	-	21.2	-
Piriformis	1	-	3.2	0.8	5.1
Rectus Femoris	2	82.1	-	81.1	13.1
Sartorius	1	-	-	-	3.4
Semimembranosus	1	-	11.4	-	-
Semitendinosus	1	-	9.1	8.8	-
Tensor Fascia Latae	1	-	-	-	6.3
Quadratus Femoris	1	-	-	-	-

Table 1. The number of strands used to replicate each muscle in the musculoskeletal model, and the muscle force in each muscle predicted by the musculoskeletal model during the separate movements of flexion, extension, adduction and abduction (– denotes forces that are below 0.1N).

Fig 1. The process of creating a digitised volumetric model from µCT scan data of a prenatal hemi-pelvic specimen, showing: (a) the initial volumetric model which contained an incomplete acetabular corpus (the triradiate cartilage is displayed in grey); (b) application of geometric morphometric method tools in AVIZO to warp an adult hemi-pelvis to the morphology of the prenatal specimen, based on the custom landmark configuration displayed by the blue spheres; and (c) the complete prenatal hemi-pelvis with reconstructed triradiate cartilage.

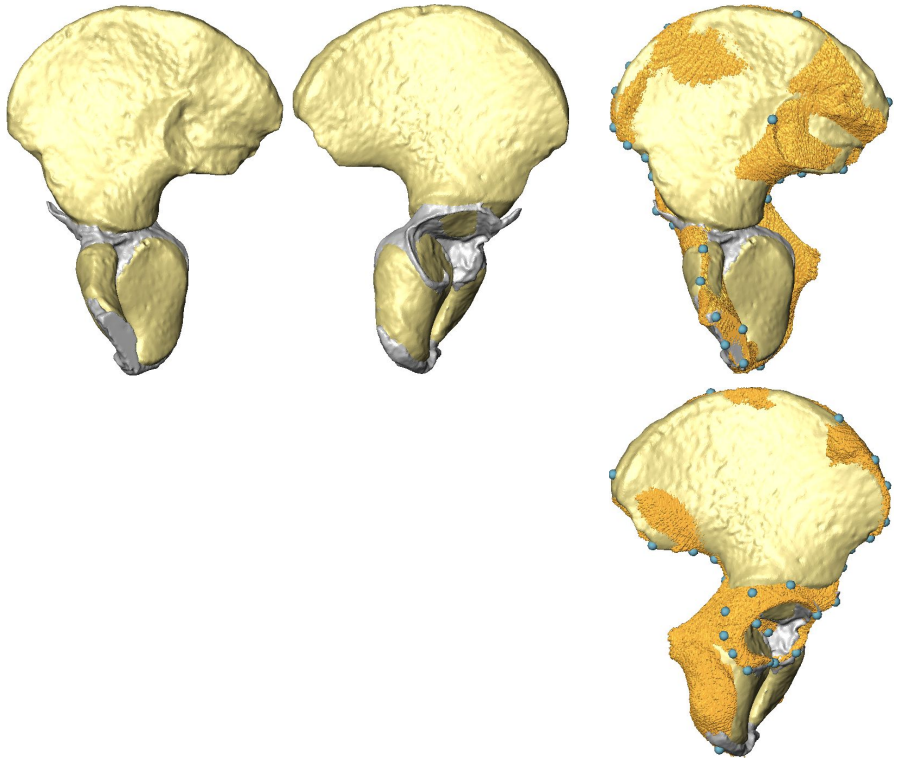

(a) **(b)**

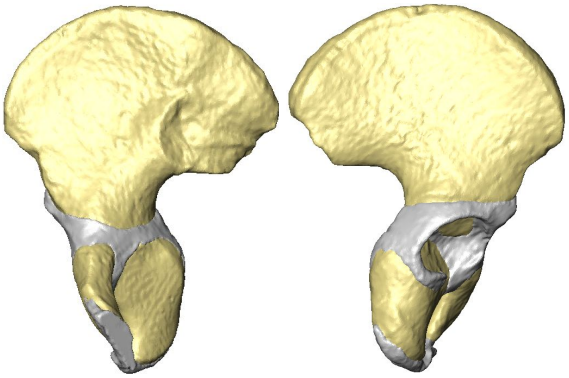

(c)

(a)

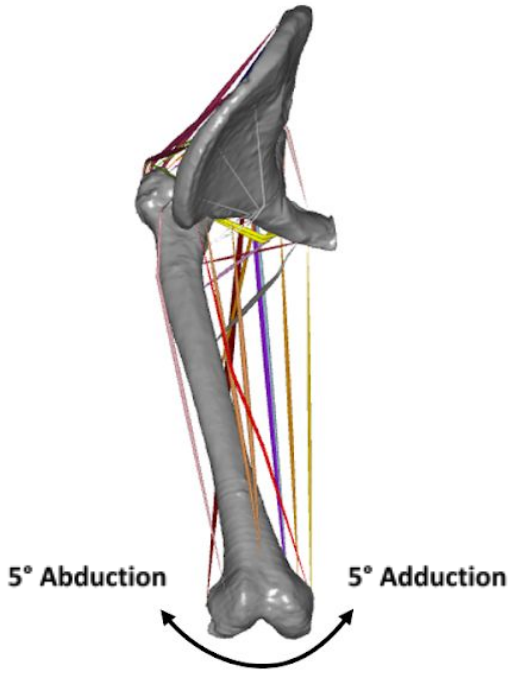

(b)

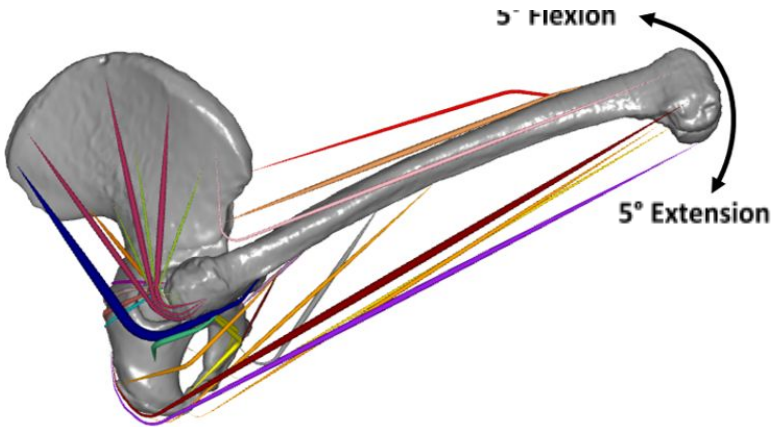

(c)

Fig 2. The musculoskeletal model of the prenatal hip which consisted of 21 muscles represented through a total of 32 individual muscle strands: (a) the initial construction of the model at a hip joint flexion of 0°; (b) a 5° adduction and 5° abduction simulated with a hip joint flexion of 110°; a further 5° flexion and 5° extension simulated with a hip joint flexion of 110°.

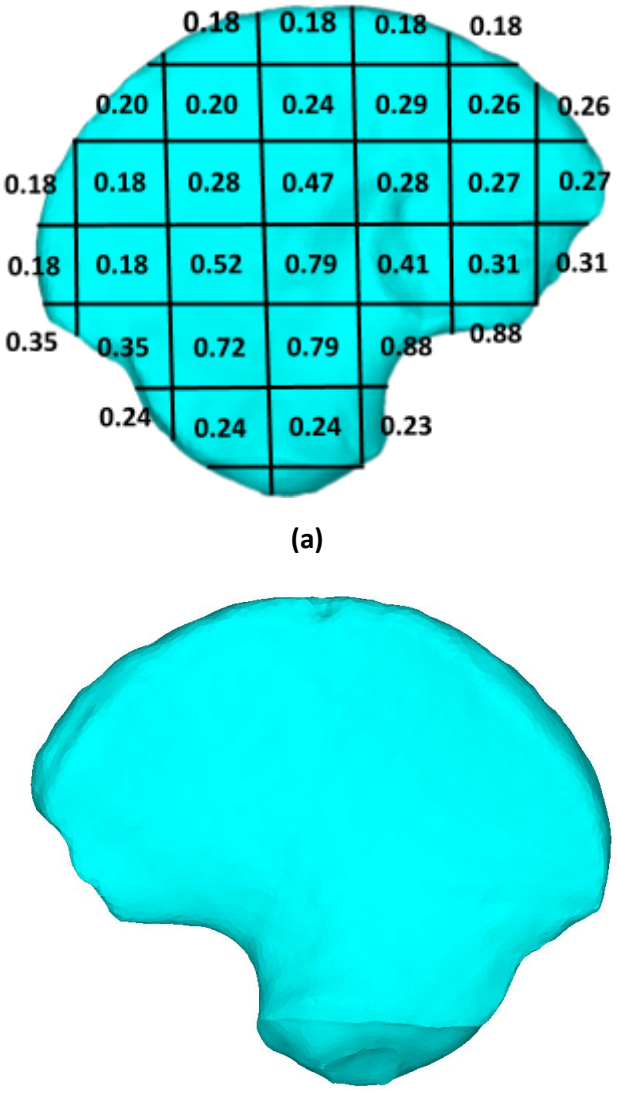

Fig 3. Modelling of the iliac cortex within the finite element model via dividing the (a) pelvic and (b) gluteal surfaces into small ROI. The thickness (mm) applied to the shell elements over each ROI are shown.

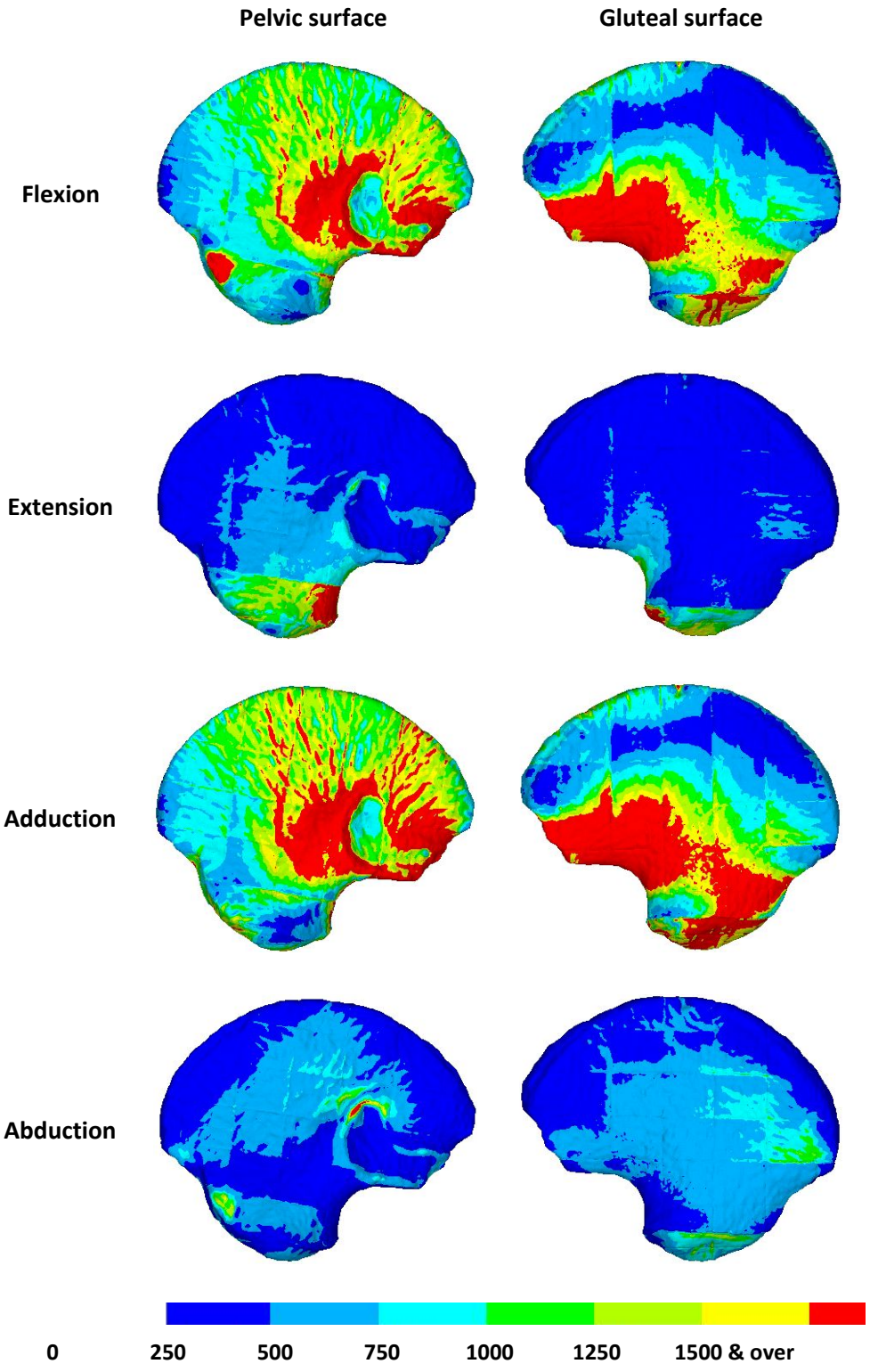

Fig 4. The distribution of the von Mises strains (μ ε) generated through four separate *in utero* movements (flexion, extension, adduction and abduction) in the ilium.

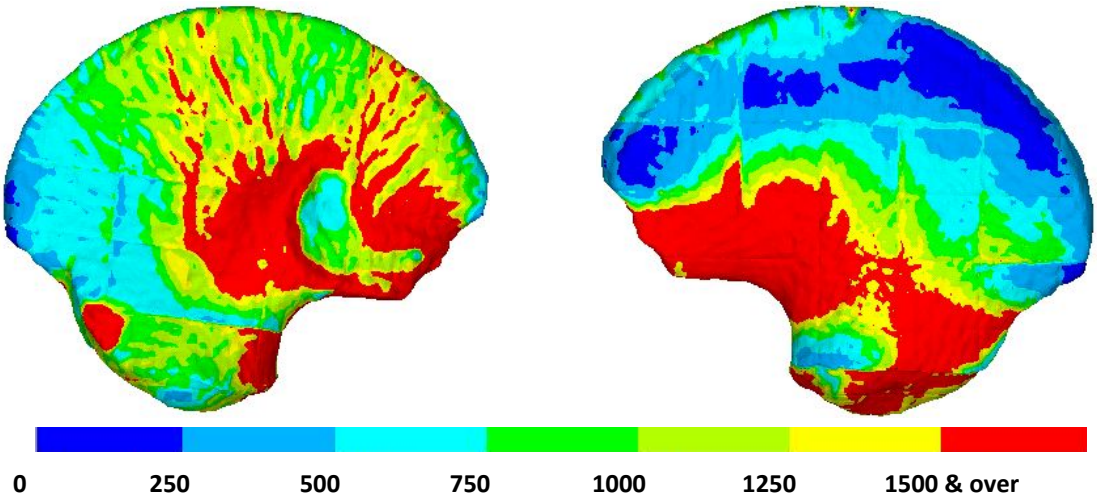

Fig 5. The distribution of the peak von Mises strain ($\mu\varepsilon$) in each element from the four separate *in utero* movements.